water

MDPI

Article

Research on the Genesis Mechanism of Hot Springs in the Middle Reaches of the Wenhe River

Cheng Xue [1], Nan Xing [1], Zongjun Gao [1,2,*], Yiru Niu [2] and Dongdong Yang [1,*]

[1] The Fifth Geological Team of Shandong Provincial Bureau of Geology & Mineral Resources, Taian 271000, China; sddkj5@126.com (C.X.); xingnan361@163.com (N.X.)
[2] College of Earth Science and Engineering, Shandong University of Science and Technology, Qingdao 266590, China; nyrsdkj@126.com
* Correspondence: zongjungao1964@163.com (Z.G.); dongyang927@163.com (D.Y.)

Abstract

This study investigates geothermal clusters in the middle reaches of the Dawen River Basin, focusing on the developmental characteristics and genetic mechanisms of typical geothermal water exposures at key sites, including Daidaoan (Taishan), Qiaogou (Culai Town), and Anjiazhuang (Feicheng). Utilizing hydrogeochemical and environmental isotope analyses, we identify a dual groundwater recharge mechanism: (1) rapid infiltration via preferential flow through fissure media and (2) slow seepage with evaporative loss along gas-bearing zones. Ion sources are influenced by water–rock interactions and positive cation exchange. The hydrochemical types of surface water and geothermal water can be divided into five categories, with little difference within the same geothermal area. The thermal reservoir temperatures range from 53.54 to 101.49 °C, with the Anjiazhuang and Qiaogou geothermal areas displaying higher temperatures than the Daidaoan area. Isotope calculations indicate that the recharge elevation ranges from 2865.76 to 4126.69 m. The proportion of cold water mixed in the shallow part is relatively large. A comparative analysis of the genetic models of the three geothermal water groups shows that they share the common feature of being controlled by fault zones. However, they differ in that the Daidao'an geothermal area in Mount Tai is of the karst spring type with a relatively low geothermal water temperature, whereas the Qiaogou geothermal area in Culai Town and the Anjiazhuang geothermal area in Feicheng are of the gravel or sandy shale spring types with a relatively high geothermal water temperature.

Keywords: geothermal water group; the middle reaches of the Wen River; hydrogeochemistry; deuterium oxygen stable isotope; thermal reservoir temperature; geothermal origin

check for updates

Academic Editor: Yijun Xu

Received: 18 June 2025
Revised: 10 August 2025
Accepted: 15 August 2025
Published: 17 August 2025

Citation: Xue, C.; Xing, N.; Gao, Z.; Niu, Y.; Yang, D. Research on the Genesis Mechanism of Hot Springs in the Middle Reaches of the Wenhe River. *Water* **2025**, *17*, 2431. https://doi.org/10.3390/w17162431

Correction Statement: This article has been republished with a minor change. The change does not affect the scientific content of the article and further details are available within the backmatter of the website version of this article.

Copyright: © 2025 by the authors. Licensee MDPI, Basel, Switzerland. This article is an open access article distributed under the terms and conditions of the Creative Commons Attribution (CC BY) license (https://creativecommons.org/licenses/by/4.0/).

1. Introduction

Geothermal energy comes from the exothermic heat of magma and the decay of radioactive elements within the Earth, and geothermal water, geothermal fields, and volcanic eruptions are the three main ways in which geothermal energy transfers energy to the Earth's surface [1]. Geothermal resources include geothermal energy, geothermal fluids, and the useful components of the Earth's interior that can be economically utilized by humans [2–4]. Geothermal energy has unique advantages, such as low cost, sustainable utilization, and environmental friendliness, and is an efficient and clean renewable energy source [5,6]. There are various types of geothermal resources. This article takes hot water-type geo-thermal resources as the main body for research. This resource is carried by liquid

water and is mainly distributed in the shallow layer of the Earth's crust. Its manifestations include hot springs and underground hot water with a temperature exceeding 25 °C that overflows the surface or is artificially excavated and extracted. Based on temperature differences, hot-water geothermal resources can be classified into three categories: high-temperature type (>150 °C), medium-temperature type (90–150 °C), and low-temperature type (≥25 °C and <90 °C). For a long time, many scholars have studied the genesis mechanism of geothermal water by means of hydrogeochemical characterization and isotopic characterization of surface water and groundwater. In the field of geothermal water research, the analytical methods of hydrogeochemistry and isotopic characteristics play an extremely crucial role. They can explain the chemical composition, circulation path, migration, and evolution process of geothermal water, as well as indicate the geological environment where geothermal water is located, and thereby derive a genesis model for geothermal water. The emergence of the Piper three-line graph provides a crucial reference basis for exploring the hydrogeochemical characteristics of geothermal water. By analyzing the content ratios of the main chemical components of geothermal water, different types of water chemistry can be identified. During the underground circulation of geothermal water, water–rock interactions occur with the surrounding rocks, causing the chemical components within the rocks to dissolve into the geothermal water. Based on the ion ratio of geothermal water and the local rock types, the sources of different water chemical types can be further analyzed. In addition, factors such as temperature, pressure and pH value simultaneously act on the evolution process of geothermal water. Isotopes in geothermal water, such as hydrogen isotopes and oxygen isotopes, are often used to trace the sources of geothermal water replenishment. Carbon isotopes, on the other hand, are applied in the age determination of geothermal water. By integrating hydrogeochemical analysis, isotopes, and the geo-logical conditions of the study area, the formation mechanism of geothermal water is inferred.

Hydrogeochemical ion ratios serve as effective tracers for elucidating water–rock interactions and characterizing cation exchange processes in aquatic systems [7]. By analyzing geothermal geological features such as heat source conditions, heat-controlling tectonics, heat storage conditions, and cover conditions in the area, the geothermal genesis model can be summarized [8]. The analysis by Peiffer et al. [9] reveals that geothermal water collected from different regions varies in water chemical types. The comprehensive application of hydrogeochemistry and stable isotopes provides new insights into thermal anomalies within rift valley systems. Deuterium-oxygen isotope tracing is a key tool for analyzing water transport pathways along the "atmosphere–vegetation–soil–groundwater" continuum through its unique fractionation effect. The deuterium-oxygen isotope tracer technique, characterized by the δD-$\delta^{18}O$ (‰) double isotope fingerprint, shows unique advantages in the analysis of hydrodynamic connections, material transport paths, and hydrological process time scales [10]. Craig [11], considering meteorological conditions, selected over 400 natural water samples from around the world and conducted research on the contents of δD and $\delta^{18}O$ in them, ultimately deriving the Craig equation. He et al. [12] collected 37 geothermal water samples from hot springs in the active tectonic area of the Sanjiang Tethys orogenic belt. Through the analysis of stable isotopes (δD and $\delta^{18}O$), they believed that the source of geothermal water replenishment in this area was atmospheric precipitation. Sun et al. [13] used isotopes such as ^{14}C to explore the genesis of geothermal fluids in the intracontinental orogenic belt at the edge of the North China Fault Depression Basin. Zhu et al. [14], based on hydrogeochemistry, conducted research on the recharge, circulation, and genesis of geothermal water in the Yinchuan Basin, which is of great significance for the sustainable development and utilization of geothermal resources. The water–rock interaction refers to the hydrogeochemical reaction caused by the difference in

chemical composition between geothermal water and the surrounding rock [15]. This interaction not only promotes the evolution process of the surface and near-surface environment, but also has an effect on the evolution of geothermal water and the stability of the stratum structure [16]. Multi-mineral equilibrium analysis, an effective approach for assessing chemical equilibrium states between geothermal fluids and reservoir minerals [17], can be employed to estimate thermal reservoir temperatures based on cation equilibrium and dissolved SiO_2 geothermometry [18]. In 1976, Muffler classified geothermal water systems into two types based on geological conditions and heat transfer methods: convective and conductive [19]. This classification method is still widely recognized today.

The middle reaches of the Wenhe River are situated in the Luzhong mountainous region of Shandong Province, an area notable for its abundant geothermal resources. The studied geothermal resources demonstrate multiple favorable attributes, including widespread reservoir distribution, diverse reservoir lithologies, moderate burial depths, abundant thermal fluid reserves, and significant development potential. These systems are predominantly characterized by low-to-medium-temperature regimes (25–150 °C), offering optimal conditions for sustainable exploitation [20,21]. Systematic exploration and evaluation initiatives launched in 1959 have, through decades of research, yielded a comprehensive understanding of key aspects, including: reservoir development characteristics in the Ludong Mountainous Hills, Lujong Mountainous Hills, and Lubei Plain regions; hydrogeochemical evolution of geothermal fluids; isotopic signatures; thermal field distribution patterns; and genetic mechanisms of the geothermal systems [22,23]. In recent years, the hydrogeological survey and special water resources development project have completed the drilling and evaluation of geothermal fields in the Luzhong mountainous area [24,25].

The study area encompasses hot spring sampling sites located along the middle reaches of the Wen River, specifically situated west of Daidaoan Hot Spring Road in Taian City, north of Qiaogou Village in Culai Town, and within Anjiazhuang Town, Feicheng City. Due to influencing factors including surface river water mixing and variable mining durations, the in situ geothermal water temperatures exhibit considerable variation, ranging from 28 °C to 54.2 °C, while closed-system measurements indicate potential reservoir temperatures reaching 80 °C. The geothermal water occurrence area lies at the junction of the Feicheng fracture basin, Dawenkou basin, and Tailai basin, with elevations ranging from 100 to 300 m. To the north is the Taishan bulge, with an elevation exceeding 1532 m; to the east is the Feedback Mountain bulge; and to the southwest is the Talesanbushan bulge. The geothermal water outcrops are distributed in the fracture zones of the Feicheng Fracture, Wenkou Fracture, and Taian–Dawangzhuang Fracture, showing obvious control by these fractures. The distribution area is small, the geothermal gradient in the overlying strata is high, and the thermal reservoir is shallow with belt-like characteristics. This study systematically investigates the geological structure and hydrogeological conditions of the study area. Through comprehensive analysis of hydrogeochemical and isotopic characteristics of geothermal fluids, we quantitatively determine the recharge elevation, thermal reservoir temperature, and origins of both water and heat sources. Furthermore, we elucidate the genetic mechanisms governing the geothermal system. The findings provide crucial hydrogeological insights to support sustainable development and utilization of local geothermal resources.

2. Materials and Methods

2.1. Overview of the Study Area

2.1.1. Geological Structure

The study area is situated in the central North China Plateau, specifically within the Luzhong Uplift of the Shandong Plateau. Geotectonically, it belongs to the Taian–Laiwu "broom-shaped" structural system, bounded by the Wengkou–Wendong Fault Zone to the south of the Lusi Fault Block Uplift and the Feicheng Fault Zone to the east. The region is topographically enclosed by the medium-high to high mountains of the Taishan Mountain System, with the Dawen River serving as the regional base level of erosion.

The formation of geothermal water in the middle reaches of the Wen River is structurally controlled by three major fault systems: the Feicheng Fault, Wunkou Fault, and Tai'an–Dawongzhuang Fault. These fault zones provide critical pathways for geothermal fluid migration and accumulation. As the base structure formed by the extrusion stress field in the Yanshan period, the northwest-trending fracture system has a significant hydrogeological demarcation role in the area. The western edge of the Tailai Basin is characterized by tensional faults such as the Daidaoan Fault, the Panghe Fault, and the Honggou Fault, which are generally NE-trending, with left-rotation strike–slip features. The Xituanshan Fault Zone in the eastern part of the Dawenkou Basin consists of several sets of tensional faults, with the Xilin–Nanliu Fault as a typical representative, and its breccia zone and fault mud constituting a regional water-resistant barrier. In the Feicheng Basin, the Story Mountain Fault, and the Mashan Fault show a southwest-trending positive fault character, controlling the contact relationship between the Cambrian–Ordovician greywacke aquifer and the Carboniferous–Diabase clastic rock layer. Such faults are generally characterized by multi-phase activation, which serves as both a demarcation mark for tectonic units and a barrier boundary for groundwater runoff.

As the most active tectonic type in the area, arc-twist tectonics are mainly developed around the fault basin. The Dawangzhuang–Tongyedian Fault Zone in the Tailai Basin has typical torsional characteristics, and the 100 m wide extrusion zone develops fault mud and tectonic breccia, forming a regional water-blocking structure. In the Feicheng Fracture Zone, the rock strata are upright and inverted, accompanied by secondary reverse faults, forming a stacked-tile tectonic system, which significantly alters the water-conducting properties of the Ordovician greywacke aquifer. The multiple activation of these structures has led to the emergence of multi-phase cemented–fragmented composite structures in the fracture zone, and their water-conducting properties show obvious anisotropy.

The porous water-bearing rock groups of loose rock types are distributed in a band-like pattern along the Dawen River system and its tributaries, featuring typical phased water storage characteristics. The Quaternary sedimentary sequence shows obvious zonal characteristics: the Shanqian alluvial sector is mainly composed of sandy clay (Shanqian Formation). The main river channel zone has developed a highly permeable gravel layer (Yihe Formation). The pore–fracture water-bearing groups of clastic rocks are mainly located in the Paleozoic to Cenozoic clastic rock series at the edge of faulted basins, and they have the characteristics of stratified fracture development. The water chemistry of this rock formation shows the transitional characteristics from HCO_3-Na-type to SO_4-Ca-type, reflecting the combined mechanism of deep circulation and shallow mixing. The fracture–karst water-bearing rock group of carbonate rocks contains two water-bearing subgroups. The karst water-bearing subgroup of pure carbonate rocks is mainly composed of the Ordovician Majiagou Group limestone and has developed multi-stage karst pipeline systems. Due to the difference in solubility, the dolomite of the Wuyangshan Formation has stratified karst development characteristics, forming a stepped water storage structure. In the karst–fracture water-bearing subgroup of carbonate rocks interbedded with clastic rocks, the

interbedded limestone and shale of the Zhangxia Formation of the Cambrian system form a unique layer–band composite water-bearing system. The water barrier boundary of the region is formed by the fractured water-bearing rock group of the magmatic metamorphic rock type and the granodiorite mass of the Archean. The development of fractures shows the characteristics of elevation zonation. The water chemical characteristics show a strong dissolution and filtration effect, with TDS values generally less than 200 mg/L, presenting typical $CaHCO_3$-type water (Figure 1).

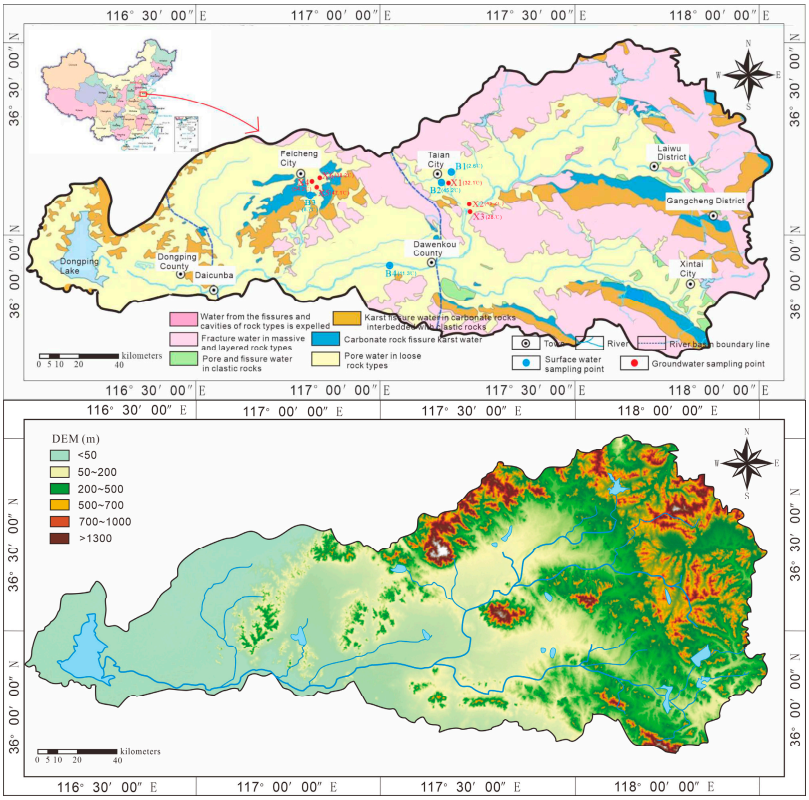


Figure 1. Schematic diagram of the location of the geothermal hot springs.

The study area's surface lithology predominantly consists of Quaternary clay deposits with well-exposed stratigraphic sequences. Based on comprehensive regional geological data, the stratigraphic framework reveals a complex geological history spanning from the Late Archean to Quaternary periods. The basement comprises metamorphic rocks of the Taishan Group, bounded by the Taikouji Formation, which primarily features biotite diorite and biotite metamorphic gneiss with minor occurrences of marble and magnetite quartzite—representing a suite of regionally metamorphosed and migmatized rocks with varying metamorphic grades. The Paleozoic marine sequences are prominently represented by well-preserved Cambrian and Ordovician formations, while the Cenozoic is characterized by terrestrial deposits. The Cambrian system exhibits a complete stratigraphic division: the Lower Cambrian includes the Wushan and Mantou Formations; the Middle Cambrian comprises the Maozhuang, Xuzhuang, and Zhangxia Formations; and the Upper Cambrian contains the Gushan, Changshan, and Fengshan Formations. Additionally, minor occurrences of Late Archean metamorphic shelly rocks and metamorphic volcanic–sedimentary rocks from the Yanlingguan Formation of the Taishan Group are present. The Quaternary deposits consist mainly of light yellow silty clay, clay, and sand layers. Hydrogeologically, the area is dominated by bedrock fissure water systems, with lateral subsurface runoff serving as the primary discharge mechanism for groundwater movement. This comprehensive lithostratigraphic assemblage reflects multiple phases of

marine transgression–regression cycles, tectonic events, and metamorphic processes that have shaped the region's geological architecture.

2.1.2. Stratum Lithology

The study area exhibits well-exposed Quaternary clay deposits at the surface, underlain by a complete stratigraphic sequence comprising Paleozoic marine sediments (Cambrian to Lower Ordovician) interbedded with continental deposits from both Paleozoic and Quaternary periods. The geological framework also includes minor Late Archean metamorphic basement rocks, representing the ancient crystalline foundation of the region. This stratigraphic assemblage records multiple phases of marine transgression–regression cycles and provides valuable insights into the tectonic evolution of the area.

2.1.3. Meteorology and Hydrology

The study area belongs to the warm temperate semi-humid monsoon climate, with typical continental climate characteristics and transitional attributes of marine climate. The thermal field shows significant seasonal differences, with an average annual temperature of 12.6 °C. The precipitation system shows strong instability, with an average annual precipitation of 689 mm. The temporal and spatial differentiation of precipitation is significant. The annual precipitation in the eastern mountainous area exceeds 800 mm, while that in the western plain is only 550 mm. Seventy percent of precipitation is concentrated from June to September.

The Dawen River system exhibits a distinctive fan-shaped drainage pattern, originating from Taizi Village at Mount Tai's southern foothills and flowing westward along the Tongyedian–Sunzu Fault Zone through the stepped geomorphological transition from central Shandong Mountains to Dongping Lake. The 9098 km^2 watershed contains 43 tributaries with catchment areas exceeding 50 km^2, forming a well-developed three-level hierarchical drainage network. In the middle reaches, the system receives substantial rainfall contributions from tributaries including the Caozhuo and Kangwang Rivers, where channel widths expand to 300–500 m, creating characteristic braided river morphology.

2.2. Sample Collection and Research Methods

In 2024, six geothermal water samples and four river water samples from the vicinity of the geothermal area were collected (Table 1). The temperature, pH, DO, and Eh were measured on site using Hach, and the temperature and pH were compared and measured using Hanna. The test results of the two instruments were basically consistent. Water was sent to Rizhao for regular ion detection (K^+, Na^+, Ca^{2+}, Mg^{2+}, F^-, Cl^-, $NO_3{}^-$, $SO_4{}^{2-}$, and $HCO_3{}^-$) (Table 2), and sent to Beijing for isotope detection (δD, $\delta^{18}O$). Stable isotopes of δD and $\delta^{18}O$ were analyzed using a stable isotope mass spectrometer (MAT 253 plus, Thermo Fisher Scientific, Waltham, MA, USA). The accuracies of the instrument in measuring δD and $\delta^{18}O$ are 2‰ and 0.2‰ respectively.

This paper uses the error of anion and cation balance to test the accuracy of water sample test data.

$$\mathrm{CBE}(\%) = \left[\frac{\Sigma\mathrm{Nc} - \Sigma\mathrm{Na}}{\Sigma\mathrm{Nc} + \Sigma\mathrm{Na}}\right] \times 100\% \quad (1)$$

In the formula: CBE represents the analytical equilibrium error, and ΣNc is the total mg equivalent of cations (meq/L). ΣNa represents the total milligram equivalent of anions (meq/L). The analysis error should be less than ±5%.

The recharge source of geothermal water was determined by isotopes, the interaction between water and rock was analyzed by hydrochemical methods, and the temperature of the thermal reservoir was estimated. The formation of each hot spring was visualized using a conceptual model diagram.

Table 1. Classification and detailed location of some sampling sites.

Type of Water Sampled	Serial Number	Temperature	Detailed Location
Surface water	B1	2.6	375 m south-west of Yanchihe Village
	B2	5.6	42 m north-east of Dongyue Mountain Resort, Taian
	B3	8.7	685 m south of Nansumi
	B4	11.3	114 m south of Dawen River
Underground water	X1	32.1	Xinhejiayuan (Hot Spring Road) west 39 m (WAHAHA)
	X2	45.2	309 m north of Qiaogou Village (Feedback Forest Hot Spring Recreation Centre)
	X3	28	332 m north of Qiaogou Village
	X4	54.2	Anjiazhuang
	X5	47.1	Anjiazhuang Hot Spring
	X6	38.2	People's Government of Anjiazhuang Township, Feicheng City

Table 2. Detection methods for element content.

Element	Testing Instrument	Instrument Model	Detection Method	Analytical Method
K^+, Na^+, Ca^{2+}, Mg^{2+}	Inductively coupled plasma emission spectrometer	Icap 7400	HJ 776-2015 (China, 2015)	Inductively coupled plasma emission spectrometry
Cl^-, $SO_4{}^{2-}$	Ion chromatograph	ICS600	HJ 84-2016 (Shenyang, China, 2016)	Ion chromatography
$HCO_3{}^-$	Burette	50 mL	DZ/T 0064.49-2021 (China, 2021)	Titration method

3. Results and Discussion

In this study, a total of ten groups of samples were collected. Specifically, two groups of samples, consisting of geothermal water and the surrounding river water, were obtained from Daidaoan in Mount Taishan, labeled as B1 and X1. In Qiaogou, Culai Town, three groups of samples were collected, which included geothermal water and the surrounding river water, and they were designated as B2, X2, and X3. Additionally, five groups of samples were gathered from Anjiazhuang in Feicheng. These samples also comprised geothermal water and the surrounding river water, and were marked as B3, X4, X5, X6, and B4.

3.1. Supply Sources

This study is based on a dataset of deuterium and oxygen isotopes in geothermal water and surrounding river water and constructs an isotope water line system in geothermal areas to reveal the evaporation and fractionation mechanisms and recharge characteristics of different water bodies (Figure 2). By comparing the global atmospheric precipitation line (GMWL) with local water cycle parameters, the controlling role of hydrological processes on isotopic composition is elucidated.

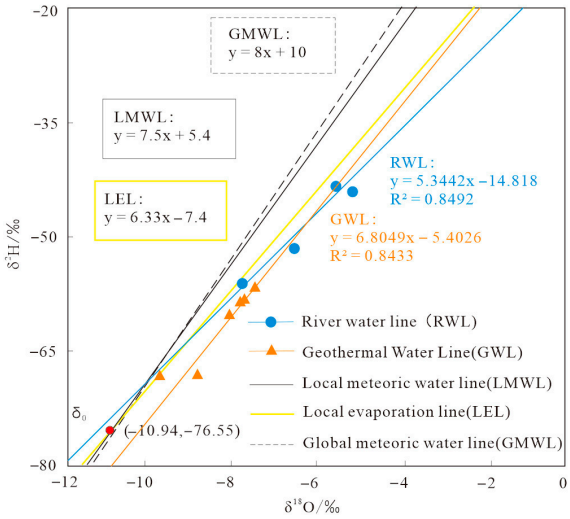


Figure 2. Deuterium oxygen isotope sites and linear fitting curves of hot springs and surrounding rivers.

The global atmospheric waterline (GMWL) formula is:

$$\delta^2H = 8\delta^{18}O + 10 \quad (2)$$

The river water line (RWL) formula is:

$$\delta^2H = 5.3442 \cdot \delta^{18}O - 14.818 \quad (3)$$

The slope and intercept are 5.3442 and −14.818, respectively, $R^2 = 0.85$.

The slope of the surface water δD-$\delta^{18}O$ relationship line is 5.3442, which is lower than the slope of GMWL by 8. This deviation is consistent with the Craig Gordon evaporation model prediction: during non-equilibrium evaporation in open water bodies, the enrichment rate of $\delta^{18}O$ is faster than that of δD, resulting in a decrease in slope. The local atmospheric waterline (LMWL) formula for the watershed is:

$$\delta^2H = 7.5 \cdot \delta^{18}O + 5.4 \quad (4)$$

Compared with GMWL, the slope decreased by 6.25%, reflecting the secondary evaporation effect of precipitation in the monsoon region, where precipitation mixed with dry air during the falling process. The intercept decreased by 46%, indicating continental climate characteristics, and the water vapor source path was transformed through inland recirculation. The local evaporation line (LEL) formula is:

$$\delta D = 6.33 \cdot \delta^{18}O - 7.4 \quad (5)$$

The slope is 6.33, which is 15.6% lower than that of LMWL, revealing the evaporation evolution law of the water body in the study area.

The formula for the groundwater line (GWL) is:

$$\delta D = 6.8049 \cdot \delta^{18}O - 5.4026 \quad (6)$$

The slope and intercept are 6.80 and −5.40, respectively, $R^2 = 0.84$.

The groundwater system exhibits unique isotopic characteristics: the mean "d-excess" is 4.53‰, significantly lower than the local atmospheric precipitation background value of 9.76‰, but higher than the surface water system by 0.78‰. This difference reveals that there is a dual mechanism for groundwater recharge, with rapid infiltration through

preferential flow in fractured media and slow leakage through evaporation losses in the unsaturated zone.

The values of δD (‰) and $\delta^{18}O$ (‰) have a certain relationship with elevation. As altitude increases, the isotopes in water decrease. It is manifested that, for every 100 m increase in altitude, δD (‰) decreases by 1.3‰ and $\delta^{18}O$ (‰) decreases by 0.3‰ [26]. The replenishment elevation was calculated by using the relationship between the δD (‰) of the atmospheric precipitation line in China and the elevation [27] (Formulas (7) and (8)). The formula is as follows:

$$\delta D = -0.02 \cdot H - 27 \quad (7)$$

$$\delta^{18}O = -0.003 \cdot H - 4.3 \quad (8)$$

In the formula, H represents the replenishment elevation. The mean values of Formulas (7) to (8) indicate that the replenishment elevation is approximately 2865.76 to 4126.69 m.

3.2. Hydrogeochemical Characteristics

3.2.1. Main Characteristics of Changes in Anions and Cations

By studying the milligram equivalent of the main components in the research area, a Schoeller logarithmic plot (Figure 3) was plotted, indicating that, except for Ca^{2+}, Mg^{2+}, and HCO_3^-, the content of other elements showed a similar trend to TDS, suggesting that they may have undergone similar water–rock interactions or have similar sources. Ca^{2+}, Mg^{2+}, and HCO_3 showed a similar trend, and there may have been carbonate decomposition.

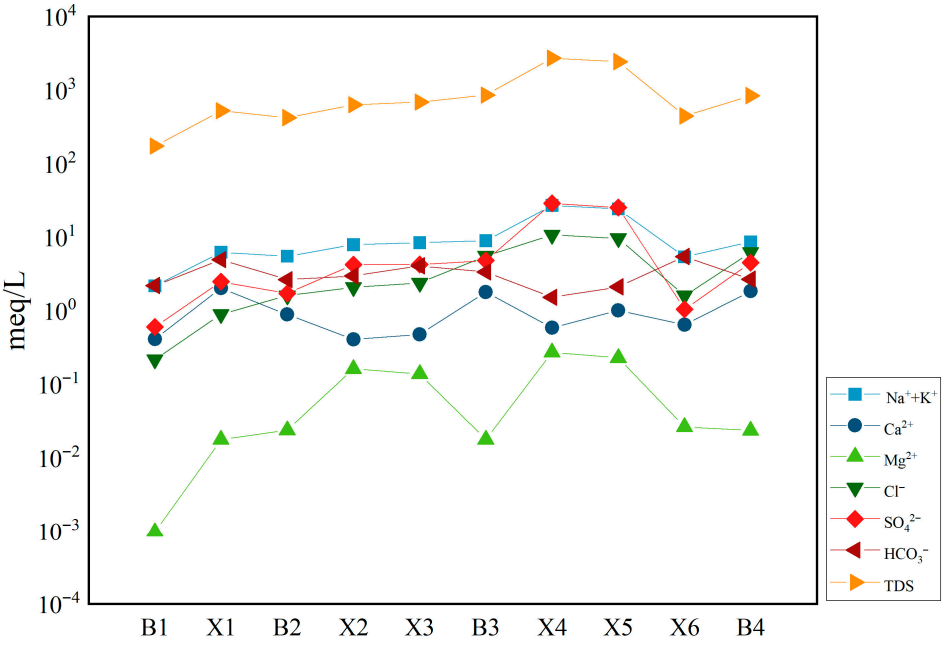


Figure 3. Schoeller logarithmic graph of chemical constant components in geothermal water and surrounding river water.

Due to the good solubility and migration ability of Na^+, both geothermal water and river water in the study area had Na^+ as the dominant cation (Figure 4), ranging from 42.37 to 279.40 mg/L. Next was Ca^{2+}, ranging from 8.17 to 40.81 mg/L. There are a large number of carbonate rocks in the research area, and it is speculated that Ca^{2+} comes from the dissolution of carbonate rocks. Figure 4 demonstrates a consistent spatial trend in cation concentrations across the three studied geothermal areas (Daidaoan, Qiaogou, and Anjiazhuang), indicating similar hydrogeochemical processes governing water–rock interactions in these systems. The significant difference in the percentage of milliequivalents of anions indicates the existence of different hydrochemical types in different water samples.

HCO_3^- ranges from 93.06 to 334.39 mg/L, SO_4^{2-} ranges from 28.92 to 1391.93 mg/L, and Cl^- ranges from 7.72 to 382.41 mg/L. Among them, B1, X1, B2, and X6 have HCO_3^- as the main anion; X2, X3, X4, and X5 have SO_4^{2-} as the dominant anion; and B3 and B4 are mainly composed of Cl^-.

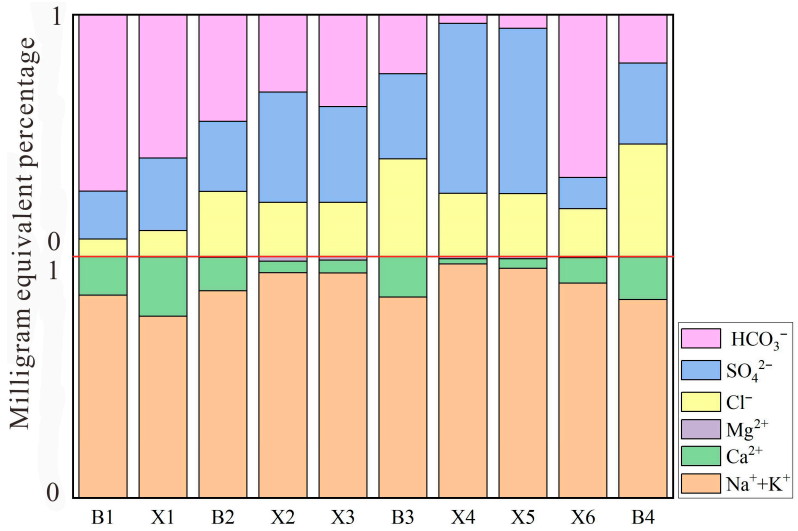


Figure 4. Percentage of milligram equivalent of the constant group.

3.2.2. Types of Water Chemistry

The Piper trilinear diagram combined with the Shukalev classification was used to determine the hydrochemical type and then analyze the evolution law of groundwater chemical composition. B1 and X6 are of HCO_3-Na-type; X1 is of $HCO_3 \cdot SO_4$ Na-type; B2 is $HCO_3 \cdot SO_4$-Cl-Na; X2 and X3 are $SO_4 \cdot HCO_3$-Na-type; B3 and B4 are $Cl \cdot SO_4$-Na-type; and X4 and X5 are SO_4·Cl-Na-type (Figure 5). It can be seen that, although there are differences in the hydrochemical types of surface water and groundwater in the same geothermal area, the overall difference is not significant, indicating that it is influenced by water–rock interactions and cation exchange.

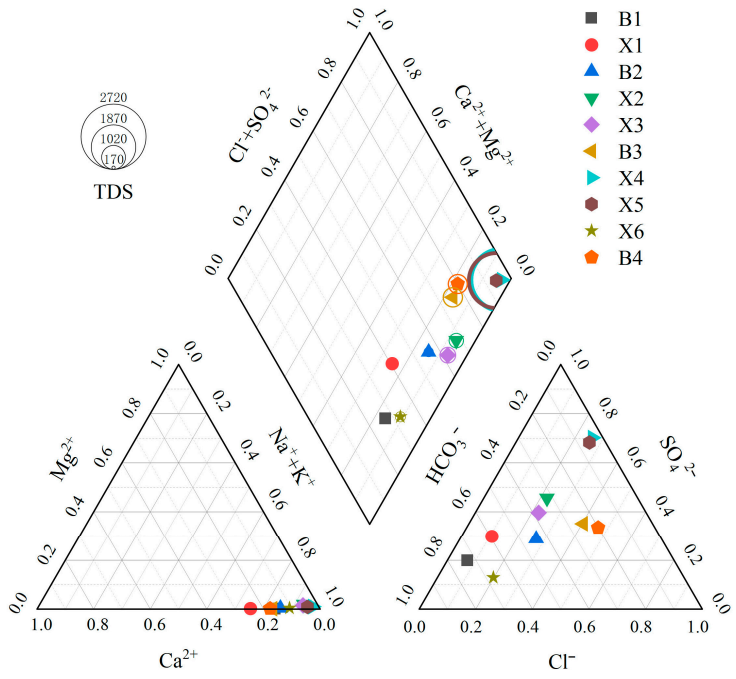


Figure 5. Piper three-line map of the hot springs and surrounding rivers.

3.3. Hydrogeochemical Ion Tracing

The chemical composition of geothermal fluids exhibits significant variation across different geological environments, with distinct ionic signatures providing critical insights into their origin and formation processes. Specific ionic ratios (e.g., Na^+/Cl^-, Ca^{2+}/Mg^{2+}) serve as reliable indicators of water–rock interaction intensity, whereas elevated concentrations of characteristic ions (such as Cl^- and SO_4^{2-}) may reflect seawater mixing influences. High-salinity geothermal waters typically form in confined aquifer systems with limited recharge, whereas low-salinity fluids often derive from open circulation systems with active meteoric water participation. Through comprehensive hydrochemical analysis of these ionic characteristics, researchers can effectively determine the genetic classification and evolutionary pathways of geothermal water systems.

Cl^- has relatively stable chemical properties, and its content is not prone to significant fluctuations. However, the stability of Na^+ is low, and water–rock interactions, cation exchange, and other factors have a significant impact on Na^+ content. Therefore, the enrichment of rock salt in geothermal water is characterized by the ratio of $\gamma(Na^+)/\gamma(Cl^-)$. As can be seen from Figure 6a, only B3 and B4 are located near y = x and may be affected by the dissolution of rock salt. However, as the study area is a karst stratum, it is considered that there is a positive cation exchange effect, which increases the Na^+ content and dissolves more Cl^- to balance it. To determine the main sources of Ca^{2+} and Mg^{2+}, the ratios of $\gamma(Ca^{2+})$, $\gamma(Mg^{2+})$, $\gamma(HCO_3^-)$, and $\gamma(SO_4^{2-})$ were analyzed. Both $(Ca^{2+}+Mg^{2+})/\gamma(HCO_3^-+SO_4^{2-})$ are less than 1, indicating the possibility of cation exchange (Figure 6b). Due to the presence of gypsum plants at sampling sites X4 and X5, the content of SO_4^{2-} may be relatively high (Figure 6b), while the remaining water samples are affected by the dissolution of carbonate rocks (Figure 6c).

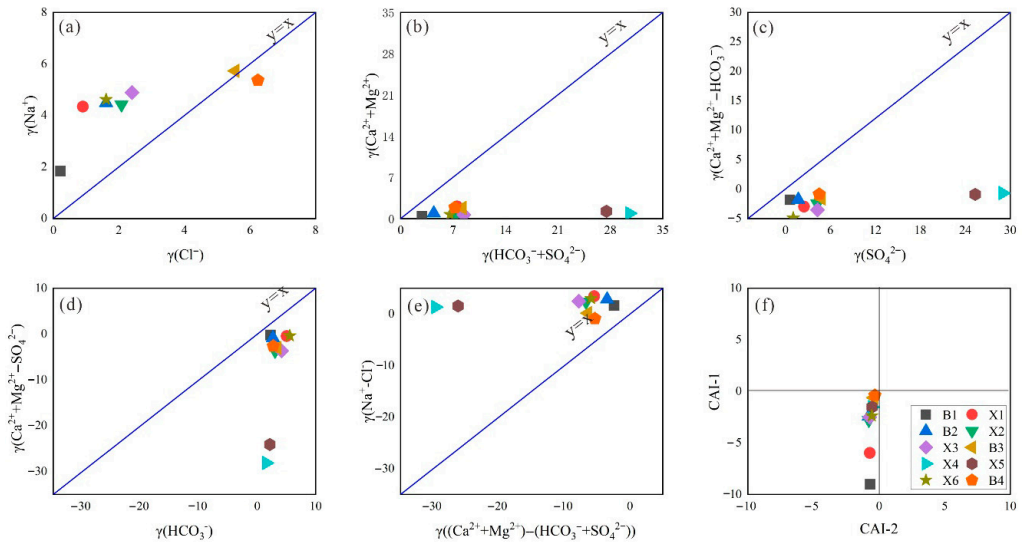


Figure 6. (**a**) $\gamma(Na^+)$ va $\gamma(Cl^-)$; (**b**) $\gamma(Ca2^+{+}Mg^{2+})$ vs $\gamma(HCO_3^-{+}SO_4^{2-})$; (**c**) $\gamma(Ca^{2+}{+}Mg^{2+}{-}HCO_3^-)$ vs $\gamma(SO_4^{2-})$; (**d**) $\gamma(Ca^{2+}{+}Mg^{2+}{-}SO_4^{2-})$ vs $\gamma(HCO_3^-)$; (**e**) $\gamma(Na^+{-}Cl^-)$ vs $\gamma((Ca2^+{+}Mg^{2+})$-$(HCO_3^-{+}SO_4^{2-}))$; (**f**) CAI-1 vs. CAI-2.

Cation exchange, also known as cation exchange adsorption, is a common phenomenon in geothermal water circulation. Minerals typically carry a negative charge and can adsorb cations from surrounding solutions. When local hot water flows through rock minerals, cations in geothermal water undergo cation exchange with cations on mineral surfaces, resulting in changes to the chemical composition of the geothermal water. Figure 6e indicates that, except for X4 and X5, the other water samples may have cation exchange interactions. The Chlor Alkali Index (CAI) is used to characterize the direction of

cation exchange. When both CAI-1 (Formula (9)) and CAI-2 (Formula (10)) are greater than 0, it indicates reverse cation exchange, and both CAI-1 and CAI-2 are less than 0. As can be seen from Figure 6f, all water samples have undergone forward ion exchange.

$$\text{CAI-1} = \left(\text{Cl}^- - \left(\text{Na}^+ + \text{K}^+\right)\right)/\text{Cl}^- \quad (9)$$

$$\text{CAI-2} = \left(\text{Cl}^- - \left(\text{Na}^+ + \text{K}^+\right)\right)/\left(\text{SO}_4^{2-} + \text{HCO}_3^- + \text{CO}_3^{2-} + \text{NO}_3^-\right) \quad (10)$$

In the formula, CAI-1 and CAI-2 represent the chloralkali index; each ion is an equivalent value for detecting ion content, meq/L.

3.4. The Genesis Mechanism of Geothermal Water Groups

The saturation index of the main rock minerals indicates that carbonate rocks are basically supersaturated. It can be determined that the geothermal water in the study area is mainly affected by the dissolution of carbonate rock salts, reflecting the characteristic that the geothermal water in the study area is karst water (Figure 7).

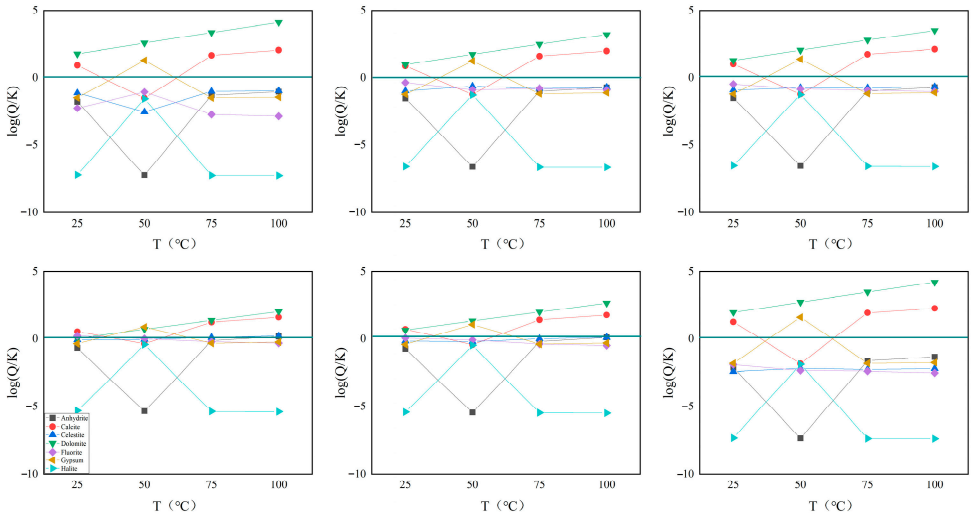


Figure 7. Saturation index map of main rock minerals.

3.4.1. Thermal Storage Temperature

There is a functional relationship between the content of dissolved substances in geothermal fluids and the temperature of the heat storage. Therefore, it is required that the content variation of the selected geothermal temperature scale should be dominated only by the single factor of temperature and have sufficient abundance. At the thermal reservoir temperature, it undergoes sufficient reaction with the surrounding rocks to achieve water–rock equilibrium. During the fluid migration process, it hardly reacts with other compounds, and there is no mixing phenomenon, or the mixing result can be calculated [28,29].

(1) Na-K Temperature scale [30,31]

$$T_g = \frac{933}{0.993 + \lg\left(\frac{\text{Na}}{\text{K}}\right)} - 273.15 \quad (11)$$

(2) K-Mg Temperature scale [32]

$$T_g = \frac{4410}{14 - \lg\left(\frac{\text{K}}{\sqrt{\text{Mg}}}\right)} - 273.15 \quad (12)$$

(3) Na-K-Ca Temperature scale [33]

$$T_g = \frac{1647}{\lg\left(\frac{Na}{K}\right) + \beta\left[\lg\left(\frac{\sqrt{Ca}}{Na}\right) + 2.06\right] + 2.47} - 273.15 \quad (13)$$

In the formula, T_g is the calculated temperature of the heat storage; Na, K, Ca, and Mg are the elemental contents, mg/L; and β is the coefficient. When T > 100 °C, β = 1/3; when T < 100 °C, β = 4/3.

The Na-K-Mg triangular equilibrium diagram is an important method for judging the cation equilibrium state in geothermal water. Giggenbach (1988) classified the water–rock equilibrium state of geothermal water into fully balanced water, partially balanced water, and immature water [33]. The cationic temperature scale method can be used when geothermal water is in a completely balanced or partially balanced state, but it is not applicable if the geothermal water is in an immature water state. Figure 8 indicates that the geothermal water groups in the middle reaches of the Wen River are all immature water. Therefore, it is not accurate to estimate the heat storage temperature using the cation temperature scale method in this study area (Table 3).

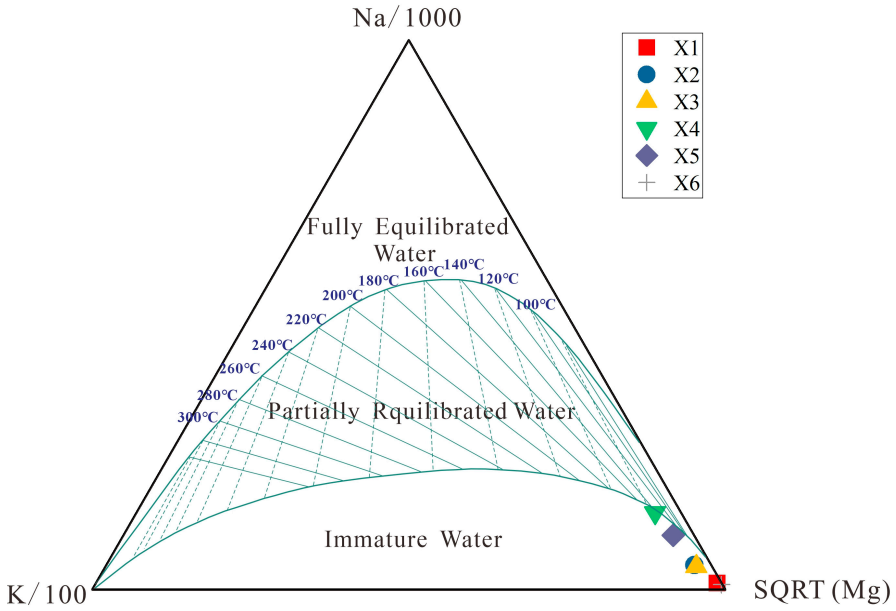


Figure 8. Na-K-Mg balance triangle diagram of hot spring.

Table 3. Estimation of thermal reservoir temperature by cationic geothermal thermometer method.

Number	Na-K (°C)	K-Mg (°C)	Na-K-Ca (β = 1/3) (°C)	Na-K-Ca (β = 4/3) (°C)
X1	151.48	38.86	131.63	40.39
X2	148.14	52.48	138.47	60.93
X3	147.70	51.77	137.75	59.49
X4	96.78	58.49	121.76	78.40
X5	105.46	55.53	125.89	78.34
X6	76.05	26.11	79.25	−9.56

The SiO_2 geothermal temperature scale is derived from the thermal reservoir temperature estimation model established by the dissolution–precipitation equilibrium of silicon-containing minerals in the water–rock system. The SiO_2 mineral has stable chemical properties and is widely present in strata. The SiO_2 dissolved in water is not prone to chemical reactions. Its solubility increases with the rise in temperature, and the mineral precipitates very slowly when the temperature drops. When estimating the temperature of

immature hydrothermal reservoirs, the SiO_2 geothermal temperature scale is more accurate than the cationic geothermal temperature scale. The common methods are as follows.

(1) Quartz temperature scale (no steam loss) [31,34]

$$T_g = \frac{1309}{5.19 - \log_{10} SiO_2} - 273.15 \quad (14)$$

(2) α-Quartz stone temperature scale [31,34]

$$T_g = \frac{1000}{4.78 - \lg SiO_2} - 273.15 \quad (15)$$

(3) Chalcedony temperature scale [31,34]

$$T_g = \frac{1032}{4.69 - \log_{10} SiO_2} - 273.15 \quad (16)$$

In the formula, T_g is the heat storage temperature, in °C; SiO_2 refers to the SiO_2 content, in mg/L.

Formulas (14) to (16) calculate that the maximum temperature of the thermal reservoir is X4 and the minimum is X1. Since the temperature calculated from the α-quartzite and chalcedony scales is lower than the measured temperature on site, they are discarded, and the quartz scale is used to calculate the heat storage temperature. The calculation of the quartz temperature scale (without steam loss) shows that the highest temperature of X4 is 101.5 °C, and the lowest temperature of X1 is 53.5 °C (Table 4).

Table 4. Estimation of geothermal temperature scale with silicon dioxide.

Number	On-Site Temperature Measurement (°C)	Quartz Temperature Scale (No Steam Loss) (°C)	a-Quartz Stone Temperature Scale (°C)	Chalcedony Temperature Scale (°C)
X1	32.1	53.5	4.9	21.1
X2	45.2	90.4	40.2	59.7
X3	28	80	30.2	48.7
X4	54.2	101.5	51.1	71.5
X5	47.1	100.7	50.4	70.7
X6	38.2	56.8	8	24.5

3.4.2. The Situation of Cold Water Mixing in

The silicon–enthalpy equation method is an idealized approach that does not take into account the energy loss caused by heat exchange between geothermal water and the surrounding rock when it rises. The mixing ratio was obtained by means of the relationship between the SiO_2 content and enthalpy [35]. To estimate the mixing ratio of cold water and geothermal water in the eastern Shandong area, the silicon–enthalpy equation method was used for calculation (Formulas (17) and (18)).

$$S_c a + S_h(1 - a) = S_s \quad (17)$$

$$SiO_{2c} b + SiO_{2h}(1 - b) = SiO_{2s} \quad (18)$$

In the formula, S_c represents the enthalpy value of near-surface cold water, ×4.1868 J/g, taken as 15 °C [29]; S_h is the initial enthalpy of deep geothermal water (Table 5), ×4.1868 J/g; and S_s is the enthalpy value of hot spring geothermal water (using the heat reservoir temperature calculated in the previous text), ×4.1868 J/g; a is the proportion of cold water mixed in based on the enthalpy value. SiO_{2c} represents the SiO_2 content in surface cold water, mg/L, with 18 mg/L taken [29]; SiO_{2h} represents the SiO_2 content in deep geothermal water

(Table 5), mg/L; and SiO_2s represents the content of SiO_2 in hot spring geothermal water, in mg/L. b is the proportion of cold water mixed in based on the content of SiO_2.

Table 5. Deep geothermal water temperature, enthalpy value, and SiO_2 content comparison table.

Temperature (°C)	Enthalpy Value (4.1868 J/g)	SiO_2 (mg/L)	Temperature (°C)	Enthalpy Value (4.1868 J/g)	SiO_2 (mg/L)
50	50	13.5	200	203.6	265
75	75	26.6	225	230.9	365
100	100.1	48	250	259.2	486
125	125.4	80	275	289	614
150	151	125	300	321	692
175	177	185	—	—	—

Based on the SiO_2 content, enthalpy value, and temperature, the cold water mixing ratio curves of a and b were plotted. The vertical coordinate of the intersection point of a and b represents the cold water mixing ratio, and the vertical coordinate represents the initial temperature of the deep geothermal water (Figure 9). The silicon–enthalpy equation method indicates that the proportion of cold water mixed with geothermal water in the Dawen River Basin is over 50% (Figure 9). The proportion of shallow cold water mixed in is relatively large, and attention should be paid to its rational development and utilization.

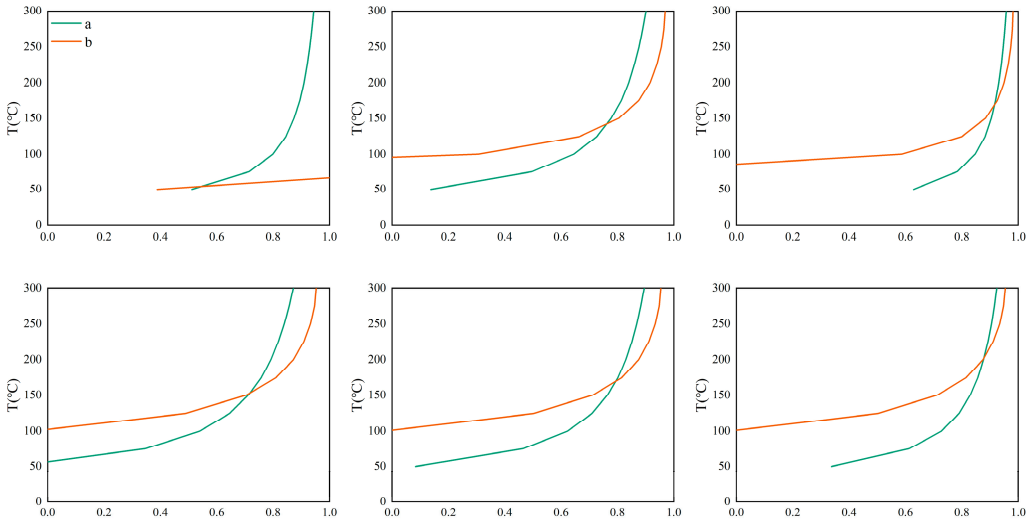


Figure 9. The proportion of cold water mixed into geothermal water.

3.4.3. The Geothermal Area of Daidao Nunnery on Tai Mount

The Taishan Daidao'an geothermal field (1.5 km^2) represents a deep-circulation convective system developing as a strip-shaped thermal reservoir within warm water resources. Located at the structural junction between the Tailai Depression and Taishan Uplift, this system is tectonically controlled by the intersection of two major fault systems: the NEE-striking Taishan Fault and NNW-trending Daidaoan Fault. The geological framework consists of Yanshanian igneous rocks formed through intense faulting and magmatic activity, underlain by Cambrian limestone hydrothermal reservoirs. These reservoirs exhibit a north-to-south roof depth variation from 200 to 800 m, characterized by complex structural conditions, poor hydrodynamic properties, and increasing ground temperatures with depth. The system's thermal dynamics are governed by fault-induced fracture zones serving as groundwater migration pathways, deep-cutting fractures connecting to heat sources, and thick shale overburden providing effective thermal insulation. Groundwater undergoes

deep convective circulation, acquiring heat before accumulating in shallow karst fissures, ultimately forming the geothermal resource at the fault intersection (Figure 10).

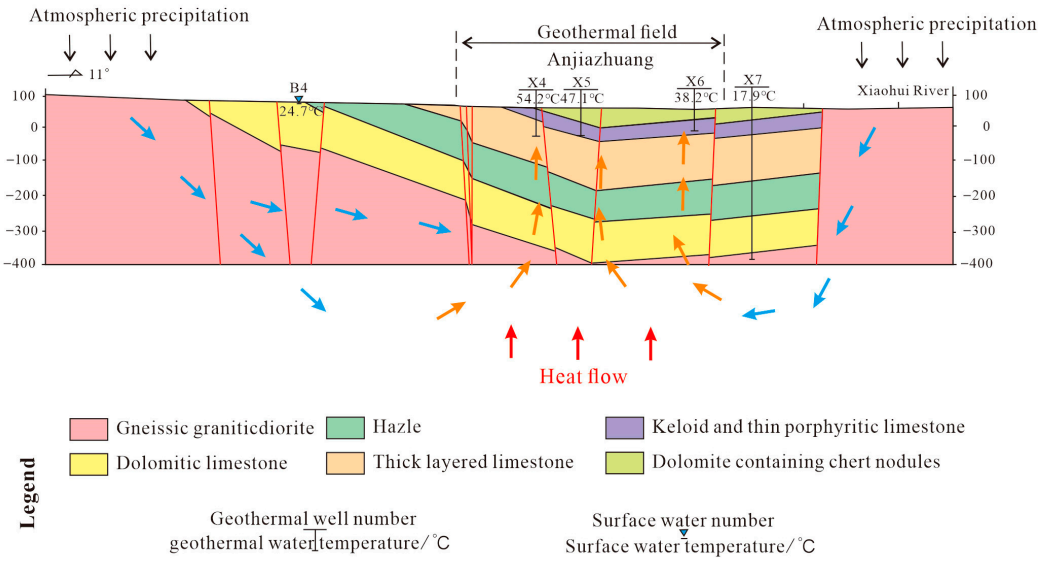


Figure 10. Conceptual diagram of the formation model of geothermal water.

3.4.4. The Qiaogou Geothermal Area of Culai Town

The Qiaogou geothermal field in Culai Town (0.30 km^2) is situated at the structural boundary between the Tailai Depression and Xinfushan Uplift, forming a banded thermal reservoir along tectonic fractures. The system develops over Neoarchean granodiorite basement that underwent intense folding, forming the Culai Mountain Complex Anticline of Mount Tai (Figure 10). The tectonic conditions are complex. The geothermal area is located in the southeast of the intersection of the Culai Mountain Fault and the Panghe Fault. The water temperature is relatively high, and the water volume is large, belonging to warm water or warm water (Figure 10).

3.4.5. The Anjiazhuang Geothermal Area in Feicheng

The study area is situated at the structural junction between the Wenkou Depression and Bushan Uplift, covering approximately 18.23 km^2. The region exhibits well-developed fault systems, among which the NNE-trending tectonic system serves as the primary thermal-controlling structure for the Anjiazhuang geothermal field (Figure 10). The thermal reservoir comprises Cambrian strata dominated by dolomite, dolomitic limestone, and marl limestone, exhibiting both banded and layered distributions. Reservoir temperatures demonstrate significant spatial variation, with the highest values occurring proximal to thermal-conductive fractures. Sand shale has good waterproofing performance, low thermal conductivity, and large thickness. When it covers the thermal reservoir, it forms a cover layer with good thermal insulation performance.

4. Conclusions

There is a dual mechanism for groundwater recharge: rapid infiltration of the preferred flow in the fissure medium and slow seepage due to evaporation loss through the gas containment zone. The types of hydrochemistry can be classified into five categories, but there is not much difference within the same geothermal area. The types of water chemistry can be classified into five categories, but within the same geothermal area, the differences in water chemistry types are not significant. Hydrogeochemical ion traceability indicates that the SI of carbonate rocks is greater than 0 and they are in a saturated state. There is

forward cation exchange in the study area. Due to the presence of a gypsum plant, the sulfate ion content in some samples is high.

This study reveals a thermal reservoir temperature range of 53.54–101.5 °C, with significant mixing of shallow cold water indicated by recharge elevations between 2865.76 and 4126.69 m. Comparative analysis shows that the Anjiazhuang and Qiaogou geothermal fields exhibit higher reservoir temperatures than the Daidaoan area. Within the Wen River mid-reach study area, extensive thermal water discharges occur along fault fracture zones. These manifestations result from complex structural features formed by multiple secondary faults in the karst terrain. The fault systems serve dual functions: as conduits for geothermal fluid migration, and as pathways for deep heat transfer.

Other reasons, such as the residual heat of magmatic activity, can be ignored due to the earlier ejection period or less distribution. In addition, the possibility of radioactive elements existing in the rock mass is relatively small, and decay energy is not considered either. Notably, the estimated reservoir temperatures at monitoring sites X1 (Daidaoan) and X6 (Anjiazhuang) were relatively low. Sustainable development strategies should be implemented for these resources to prevent overexploitation and ensure long-term utilization.

Author Contributions: Conceptualization, Z.G. and C.X.; methodology, Z.G. and Y.N.; software, Y.N.; validation, N.X.; formal analysis, D.Y.; investigation, Z.G. and Y.N.; resources, C.X. and N.X.; data curation, Y.N.; writing—original draft preparation, Z.G. and Y.N.; writing—review and editing, Z.G. and C.X.; visualization, Y.N.; supervision, D.Y.; project administration, C.X. and D.Y.; funding acquisition, C.X. and N.X. All authors have read and agreed to the published version of the manuscript.

Funding: This research received no external funding.

Data Availability Statement: The data presented in this study are available on request from the corresponding author.

Acknowledgments: Thank you to the editor for the efforts made for the publication of this article and to the reviewers for their revision suggestions.

Conflicts of Interest: The authors declare no conflicts of interest.

References

1. Guo, Q.; Pang, Z.; Wang, Y.; Tian, J. Fluid geochemistry and geothermometry applications of the Kangding high-temperature geothermal system in eastern Himalayas. *Appl. Geochem.* **2017**, *81*, 63–75. [CrossRef]
2. Wang, G.; Zhang, W.; Liang, J.; Lin, W.; Liu, Z.; Wang, W. Evaluation of Geothermal Resources Potential in China. *Acta Geosci. Sin.* **2017**, *38*, 449–450+134+451–459. (In Chinese)
3. Shi, Q.; Fan, J.; Shi, F.; Wang, X.; Zheng, H.; Meng, J.; Song, S. Potential evaluation and development utilization technology of geothermal resources in the Jining Coalfield. *Chin. J. Eng.* **2025**, *47*, 1137–1150. (In Chinese)
4. Sun, G. Study on the Characteristics and Formation Mechanism for Typical Geothermal Systems of a Railway in Southeastern Tibet. Master's Thesis, Southwest Jiaotong University, Sichuan, China, 2022. (In Chinese).
5. Wang, Z.; Shen, L.C.; Liang, Z.B.; Jiang, Z.L.; Liao, Y. Characteristics of Hydrochemical Compositions and Stable Carbon Isotope of Natural Water in the Daggyia Geothermal Field, Tibet, China. *Carsologica Sin.* **2015**, *34*, 201–208. (In Chinese)
6. Pang, Z.; Kong, Y.; Shao, H.; Kolditz, O. Progress and perspectives of geothermal energy studies in China: From shallow to deep systems. *Environ. Earth Sci.* **2018**, *77*, 580. [CrossRef]
7. Feng, N.; Qin, X.; Ma, Y.; Wang, B.; Jiang, Z.; Zhang, F.; Liu, R.; Qin, X. Environmental geochemical characteristics and quality evaluation of hot spring in Reshui Township, Dulan County, Qinghai Province. *Geol. Bull. China* **2025**, 1–16. Available online: https://link.cnki.net/urlid/11.4648.P.20250320.1043.004 (accessed on 17 June 2025). (In Chinese)
8. Fang, Y. Research on the geothermal genesis model of Bantang hot spring area, Chaohu City. *Groundwater* **2025**, *47*, 26–29. (In Chinese)
9. Peiffer, L.; Inguaggiato, C.; Wurl, J.; Fletcher, J.M.; Martínez, M.G.O.; Martínez, D.C.; Legrand, D.; Hernández-Morales, P.; Reinoza, C.E.; Tchamabé, B.C.; et al. Geochemistry of Coastal Geothermal Systems from Southern Baja California Peninsula (Mexico): Fluid Origins, Water-rock Interaction and Tectonics. *Chem. Geol.* **2024**, *670*, 122316. [CrossRef]
10. Wang, J.; Chen, J.; Lu, B.; Tong, H.; Tan, Z.; Sun, Y.; Lin, T.; Wang, Y. Some Reviews and Prospects of Isotopic Hydrology. *J. Hohai Univ. (Nat. Sci. Ed.)* **2015**, *43*, 406–413.

11. Craig, H. Isotopic Variations in Meteoric Waters. *Science* **1961**, *133*, 1702–1703. [CrossRef]
12. He, P.; Zhang, H.; Li, S.; Zhou, X.; Zhou, X.; He, M.; Tian, J.; Zhang, Y.; Wu, Z.; Chen, T.; et al. Geological and Hydrochemical Controls on Water Chemistry and Stable Isotopes of Hot Springs in the Three Parallel Rivers Region, Southeast Tibetan Plateau: The Genesis of Geothermal waters. *Sci. Total Environ.* **2024**, *906*, 167648. [CrossRef] [PubMed]
13. Sun, H.; Sun, X.; Wei, X.; Huang, X.; Ke, G.; Wei, H. Geochemical Characteristics and Origin of Nuanquanzi Geothermal Water in Yudaokou, Chengde, Hebei, North China. *J. Earth Sci.* **2023**, *34*, 838–856. [CrossRef]
14. Zhu, Y.; Yang, Q.; Chang, X.; Hao, W.; Ma, Y.; Martín, J.D. A Hydrogeochemical and Isotopic Approach for Assessing the Origin, Recharge and Mixing Process of Geothermal Water in the Yinchuan Basin. *J. Geochem. Explor.* **2025**, *269*, 107636. [CrossRef]
15. Redwan, M.; Abdel, M.; Abo, A. Effect of Water–rock Interaction Processes on the Hydrogeochemistry of Groundwater West of Sohag Area, Egypt. *Arab. J. Geosci.* **2016**, *9*, 111. [CrossRef]
16. Shen, Z.; Wang, Y.; Guo, H. Opportunities and Challenges of Water-Rock Interaction Studies. *Earth Sci.* **2012**, *37*, 207–219. (In Chinese)
17. Hai, K. Using Several Methods to Estimate the Temperatures of Deep Geothermal Reservoirs. Master's Thesis, University of Geosciences, Beijing, China, 2019. (In Chinese)
18. Zheng, Y.; Li, X.; Bai, Y.; Hou, H.; Yao, Z.; Yan, Y. Chemical Characteristics and Genesis Analysis of Hot Spring Water in Shangri-La Area. *Water Resour. Prot.* **2024**, *40*, 158–164.
19. Muffler, L. Tectonic and Hydrologic Control of the Nature and Distribution of Geothermal Resources. *Geo-Heat Cent. Q. Bull.* **1976**, *15*, 499–507.
20. Luo, W.Q.; Zhang, S.K.; Yu, X.F.; Tian, J.X.; Yang, B.; Zhang, Y.; Chen, J.; Ma, X.X.; Tang, L.L.; Sun, X.Z. Review on Research Progress of Yishu Fault Zone. *Shandong Land Resour.* **2018**, *34*, 59–65. (In Chinese)
21. Wang, X.; Zhong, D.; Li, L. Discussion on the Evolution Relationship and Dynamic Background of the Late Mesozoic between the Westward Fault System in Northwest Shandong and the Yishu Fault Zone. *Earth Sci. Front.* **2010**, *17*, 166–190. (In Chinese)
22. Zhao, J. *Study on the Spatial Structure of Deep Thermal Storage and the Process of Hydrothermal Differentiation in Xiongan New Area*; Chinese Academy of Geological Sciences: Beijing, China, 2020. (In Chinese)
23. Gao, Z.; Li, S. The Renewal Capacity in Geothermal Water in North China. *Sci. Technol. Vis.* **2014**, *34*, 73–74. (In Chinese)
24. Cai, Y.; Zhong, X. Overview of Typical Geothermal Fields in the Central and southern part of Shandong Province. *Land Resour. Shandong* **2015**, *31*, 24–30. (In Chinese)
25. Liu, Y.; Zhang, T.; Meng, M.; Zhang, H.; Liu, P.; Li, X.; Du, Y. Characteristics of Geothermal Resource Zoning and Geothermal Field Division in Shandong Province. *Coal Geol. China* **2024**, *36*, 33–37. (In Chinese)
26. Yu, J.; Yu, F.; Liu, D. The Oxygen and Hydrogen Isotopic Compositions of Meteoric Waters in the Eastrn Part of China. *Geochimica* **1987**, *1*, 22–26. (In Chinese)
27. Wang, K.; Wang, D. Application of Environmental Isotopes to Studies of the Origin and Recharge Mechanism of Geothermal Water. *Geol. Rev.* **2002**, 203–209. (In Chinese) [CrossRef]
28. Liu, Y.; Zhou, L.; Lv, L.; Li, W.; Wang, X.; Deng, Q.; Song, M.; Zheng, Y.; Ma, X. Geothermal geological characteristics and hot water genesis in the mountainous areas of central Shandong. *Geol. Bull. China* **2020**, *39*, 1908–1918. (In Chinese)
29. Wang, X. A Study of the Characteristics and Genesis of the Hot Springs in the Western Shandong Peninsula. Master's Thesis, China University of Geosciences, Beijing, China, 2018. (In Chinese)
30. Fournier, R.O.; Truesdell, A.H. An Empirical Na-K-Ca Geothermometer for Natural Water. *Geochim. Cosmochim. Acta* **1973**, *37*, 1255–1257. [CrossRef]
31. Liu, M. Study of Occurrence Characteristics and Formation Model of Ceothermal Water in Shandong Province. Master's Thesis, Shandong University of Science and Technology, Qingdao, China, 2022. (In Chinese)
32. Tian, Y. Research on the Formation Mode of Geothermal Energy and the Genesis Types of Geothermal Water in Shandong Province. Master's Thesis, Shandong University of Science and Technology, Qingdao, China, 2013. (In Chinese)
33. Huang, H.; Yuan, X.; Peng, Q.; Guo, Y.; Xue, Z.; Dan, Z.; Li, J.; Liu, Z.; Ba, S.; Sun, F.; et al. Geochemical characteristics and Genesis Mechanism of Geothermal Water and Traverage in the Southern Himalayas. *Sediment. Tethys Geol.* **2023**, *43*, 340–356. (In Chinese)
34. Truesdell, A.H.; Fournier, R.O. Procedure for Estimating the Temperature of a Hot Water Component in a Mixed Water Using a Plot of Dissolved Silica vs Enthalpy. *J. Res. U.S. Geol. Surv.* **1977**, *5*, 49–52.
35. Xiao, Y.; Mo, P.; Zhang, J.; Zhao, X.; Li, J.; Zhang, P.; Li, F. A New Viewpoint Concerning Genesis of Karst thermal Groundwater Under Cold-hot Water Mixing. *J. Eng. Geol.* **2021**, *29*, 383–393. (In Chinese)

Disclaimer/Publisher's Note: The statements, opinions and data contained in all publications are solely those of the individual author(s) and contributor(s) and not of MDPI and/or the editor(s). MDPI and/or the editor(s) disclaim responsibility for any injury to people or property resulting from any ideas, methods, instructions or products referred to in the content.